Topology Optimization of a Wideband Planar Phased Array Element using Periodic Level Set Functions

Christopher T. Howard*†, Alex Saad-Falcon†, David W. Landgren*, and Kenneth W. Allen*†
*Advanced Concepts Laboratory
Georgia Tech Research Institute, Atlanta, GA, 30332-0866
Email: christopher.howard@gtri.gatech.edu
†School of Electrical and Computer Engineering
Georgia Institute of Technology, Atlanta, GA 30332–0250
Email: alexsaadfalcon@gatech.edu

2024 IEEE International Symposium on Phased Array Systems and Technology (ARRAY) | 979-8-3503-9214-2/24/$31.00 ©2024 IEEE | DOI: 10.1109/ARRAY58370.2024.10880330

***Abstract*—Adding complexity to the radiating surface of a planar phased array has the potential to extend the bandwidth of economical array designs, while allowing relative trade-offs between broadside gain, scan volume, and polarization purity to be more fully explored. This work introduces the use of the periodic level set function (p-LSF) for antenna arrays, an approach which can describe complex material distributions through only a few continuously variable parameters, and applies it to the optimization of a broadband, single polarization, and unbalanced phased array element. The optimization and resulting element are compared against similar prior optimizations of a fragmented aperture antenna with equivalent bandwidth requirements. Finally, the scan performance of an 18x18 finite array (16x16 driven) with the optimized element is modeled and shown.**

***Index Terms*—phased arrays, planar arrays, level set, genetic algorithms, broadband antennas, finite difference methods**

I. Introduction

Choice of element is a crucial step in the development of a phased array system; while the element may not occupy the majority of the size, weight, or cost of any system, it plays an outsized role in defining system performance. After all, no level of quality in array electronics can overcome an element with a poor element factor and an imperfect match. A variety of element topologies have been proposed to enhance the bandwidth and scan performance of phased array systems, including the planar ultrawideband modular antenna (PUMA) array [1], the balanced antipodal Vivaldi antenna (BAVA) array, the frequency-scaled ultrawide spectrum element (FUSE) array [2], fully-planar inverted-L monopole (FILM) array [3], and the interwoven spiral array (ISPA) [4]. A common feature of these antenna types is increased mutual coupling between adjacent array elements, which provides a wide bandwidth by producing an approximately uniform current sheet on a plane, rather than by exciting currents in isolated resonant elements.

In this work, we aim to produce a wideband planar array on a single-layer printed circuit board driven by an unbalanced feed over a ground plane. This design constraint precludes many of the defining features of successful ultra wideband antennas, such as the shorting posts of the PUMA or integrated baluns of the TCDA, meaning that any improvements in bandwidth must come from variation in the distribution of metal on the radiating surface. A typical optimization strategy is to choose some canonical shape for that metal distribution, such a bowtie, dipole, or patch, then parameterize its relevant dimensions and allow those to be continuously varied by the optimizer [5], [6]. This places overly narrow constraints on the distribution of metal, however – a design objective best met by some element shape somewhere between a triangular bowtie and a rectangular patch will never be considered by the optimizer.

Topology optimization – the process of distributing material in a design space to produce desired physical properties [7] – has been applied in various fields, primarily structural design, where finite element analysis (FEA) is used to evaluate possible material distributions against some objective function. The most general approach allows each location in discretized space to toggle between two different materials; however, this tends toward an optimization with an impracticably large number of free variables, many with little impact on the quality of the final design. In order to make the optimization tractable, regions of space – pixels or fragments – must be grouped together, a technique equivalent to that which produces the fragmented aperture array [8]. In this work, we explore applying level set functions for phased array antenna element optimization in direct comparison to this fragmented approach as a point of reference for a well known optimization technique.

II. Periodic Level Set Function for Arrays

A. Periodic Level Set Function

The arrangement of metal on a surface is necessarily a binary problem; at each point in space, metal either exists or it does not. It is therefore natural to consider an optimization scheme, such as the fragmented basis, which toggles the existence of metal at predefined locations. Yet the performance of an antenna is rarely greatly affected by a particular location

979-8-3503-9214-2/24/$31.00 © 2024 IEEE

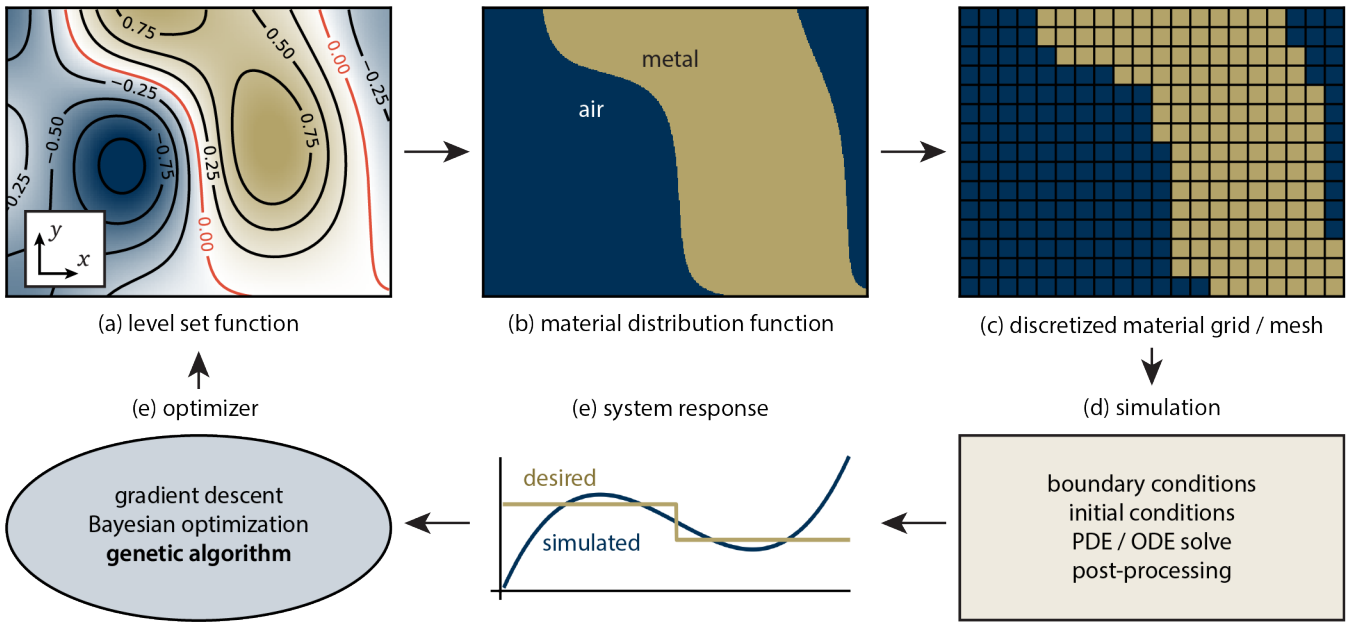

Fig. 1. A flowchart illustrating a basic topology optimization routine. (**a**) The level set function produces a smooth topology of hills and valleys. (**b**) Arrangement of metal on the surface is determined by the points on the LSF above the zero level. (**c**) The material distribution function must be discretized for use in a computational electromagnetic simulation. (**d**) Some example steps used to simulate the material distribution and evaluate its physical properties. (**e**) A comparison between the actual system response for the material distribution function and the desired system response. (**f**) After results are fed into an optimization algorithm, the optimizer suggests a new level set function to evaluate.

in the unit cell having metal or not; rather, by that location being part of broader region of metal or air which is of the right shape or size and is connected properly to other regions. An expressive mapping of optimization parameters to the distribution of metal should therefore allow regions of metal to grown and shrink as the parameters change. This is the rationale for the level set method. Consider a level set function (LSF) $f_{\boldsymbol{\alpha}}$ composed of a sum of N Gaussian radial basis functions (RBFs)

$$f_{\boldsymbol{\alpha}}(\boldsymbol{x}) = \sum_{i=1}^{N} \alpha_i \exp\left(-\frac{\|\boldsymbol{x} - \boldsymbol{c}_i\|_p^2}{2\sigma_i^2}\right) \tag{1}$$

where the i-th RBF has a fixed center $\boldsymbol{c}_i$ and variance σ_i, and $\|\cdot\|_p$ is a p-norm distance function with $p = 2$. The RBF centers are evenly spaced across the 2D unit cell, such that $\boldsymbol{x} = (x, y)$, and are weighted by coefficients $\alpha_i \in [-1, 1]$. Regions of metal are determined by the material distribution function

$$\rho_{\boldsymbol{\alpha}}(x, y) = \begin{cases} \text{metal}, & \text{if } f_{\boldsymbol{\alpha}}(x, y) \geq T \\ \text{air}, & \text{otherwise} \end{cases} \tag{2}$$

where T is the threshold value, typically $T = 0$. The weighting of basis functions, which can be controlled by the optimization scheme, determines the elevation of a smooth topographical profile, and any locations with elevation above the threshold value are assigned to be metal. Increasing the value of any coefficient will cause regions of metal to expand. A graphical depiction of this process in context of an optimization design flow is shown in Fig. 1.

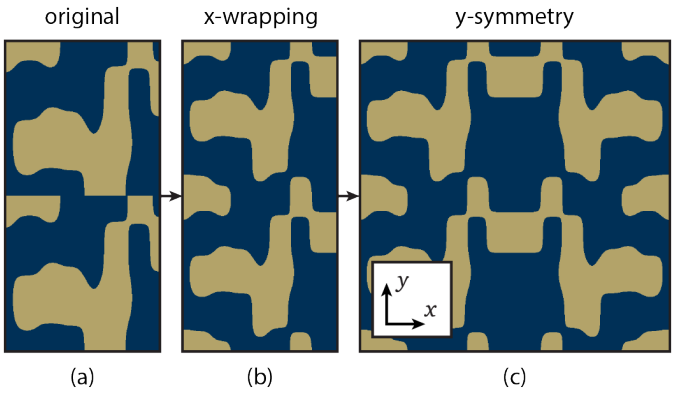

Fig. 2. An example for taking (a) an arbitrary material template on a periodic surface and applying (b) wrapping and (c) symmetry in the vertical and horizontal directions, respectively.

A few modifications of this definition are necessary to apply the LSF to the design of a periodic antenna element. First, the periodic LSF (p-LSF) is defined by allowing the distance norm in (1) to wrap around the unit cell boundary, as detailed in [9]; this ensures no sharp discontinuities exist at the periodic boundary. Second, antenna designs frequently benefit from some form of symmetry, both to reduce complexity and to reduce cross-polarization. These modifications are combined and illustrated in Fig. 2. Periodic wrapping is employed in the y boundary while mirror symmetry is enforced in the x direction which induces smoothness without wrapping. Finally, the LSF is capable of producing fine spatial features

which cannot be realized by relevant fabrication processes; an erosion and dilation approach is applied to enforce the fabrication constraints of minimum trace/gap width on the material distribution function [10].

B. Comparison to Patch Elements

One immediate question which deserves attention is whether a unit cell parameterized in this way could be capable of producing a canonical element; that is, if simple designs such as the inverted-L or patch would be produced by an optimizer if those designs were in fact optimal for a particular design objective. The ability of the LSF to synthesize various sizes of patch element is shown in Fig. 3. For each patch size, the coefficients to generate the closest match from an LSF with 32 basis functions are computed using a pseudo-inverse sampling technique [9]. Each are modeled as an element in an infinite array, spaced over a ground plane by a 3.05 mm substrate ($\varepsilon_r = 3.0$) and fed by an off-center unbalanced feed. For several patch widths, the voltage standing-wave ratios (VSWRs) for the patch and its equivalent LSF element are shown to produce similar bandwidths. The granularity in width control shown in this figure would require a minimum of 162 pixels (9x18 with reflection symmetry) in a fragmented basis to identically recreate the patch; even so, patch dimensions between the demonstrated values could be interpolated by the level set function while the fragmented basis could only select discrete patch widths.

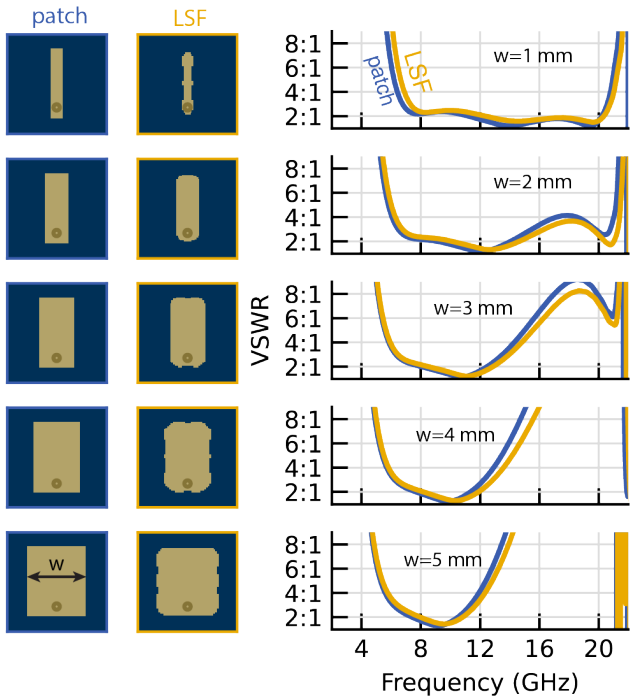

Fig. 3. The LSF is able with the appropriate coefficients to realize a continuous range of patch sizes. Each row shows from left to right a patch periodic element, the closest element realizable by an 8x8 LSF with left-right symmetry (32 basis functions), and a comparison between the VSWRs of each.

III. Optimization of a Phased Array Element

A. Genetic Algorithm Optimization

The level set function is amenable to a variety of different optimization strategies. One advantage of the LSF is that the distribution of material changes smoothly with the LSF parameters, which can lead to an improved optimization landscape, and a gradient of the parametric space can be readily computed. However, due to the complexity of the relationship between basis coefficients and the resulting electromagnetic fields, gradient-free optimization algorithms offer the most flexibility for applying the LSF technique to any class of electromagnetic design. More advanced techniques, such as inverse design, potentially offer greater optimization efficiency [11], but must be tailored to a particular class of problems during the setup phase of the design.

Genetic algorithms (GAs) have seen frequent use in array design [12]–[15]. Inspired by the evolutionary principle of natural selection, these algorithms maintain a population of individuals from whom offspring are created with mutation and crossover and evaluated against some fitness function. Individuals scoring higher on the fitness function than individuals in the population are added to the population, and poorly performing individuals are discarded. GAs have been shown to be robust in solution spaces where many local extrema may hamper gradient descent approaches.

Since bandwidth is the primary target for this optimization, a suitable fitness function must evaluate relevant performance metrics, such as gain or return loss, over a range of frequency points and penalize any frequencies which do not meet the predetermined goal. A generalized mean ($p = 8$) is used to penalize designs which have frequency points which perform very poorly compared to designs where a greater bandwidth is close to spec. In other words, a broadband design which performs slightly worse than desirable across the entire specified band will be preferred over a design which performances very well over much of the band, but poorly over the rest. The fitness function is defined as follows: for some goal $g(f)$ over frequency f, specified as a piecewise linear function, the penalty function for simulated performance $s(f)$ when the goal is for s to exceed g is

$$\mathcal{F}_{s>g} = \left(\frac{1}{N} \sum_{i=1}^{N} \min\{s(f_i) - g(f_i),\ 0\}^p \right)^{1/p} \tag{3}$$

where N is the number of frequency points obtained from the simulation. A similar formulation ($\min\{g - s,\ 0\}$) is used for $\mathcal{F}_{s<g}$, when the result should be less than the goal. The element optimizations for the design simultaneously minimize reflection coefficient and maximize element efficiency, for a total fitness function of

$$\mathcal{F}_{\text{total}} = \frac{1}{2} \left(\mathcal{F}_{\Gamma_{\text{db}} < \Gamma_{\text{goal}}} + \mathcal{F}_{\eta_{\text{db}} > \eta_{\text{goal}}} \right) \tag{4}$$

Reflection coefficient Γ_{db} and efficiency η_{db} are obtained from an in-house finite-difference time-domain (FDTD) solver with periodic boundary conditions to simulate the element's

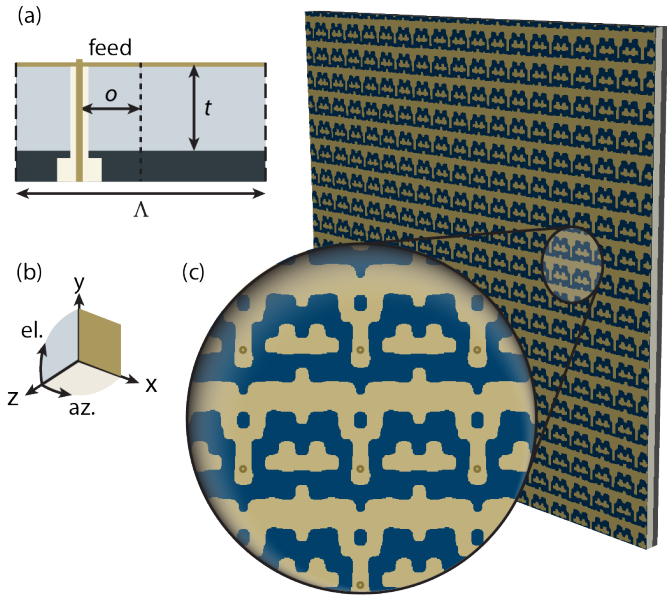

Fig. 4. The connected array element produced by periodic level set function (p-LSF) optimization. (a) Relevant dimensions of the design: the feed offset o and the substrate thickness t. (b) Coordinate definitions for the array. (c) The periodic element pattern.

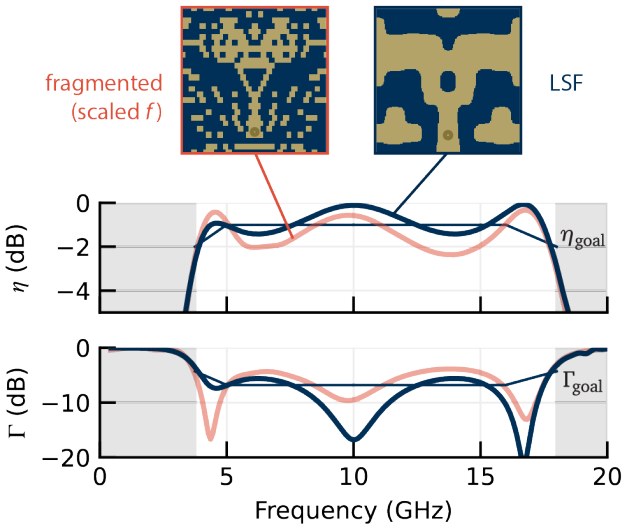

Fig. 5. Infinite array efficiency η and return loss Γ for the optimized LSF element, compared to the the fragmented aperture optimized in a previous work [17]. The frequency of the fragmented array (a larger element) is scaled to match the desired band of the LSF array.

presence in an infinite array. The goals for each element are listed in Table I.

TABLE I
OBJECTIVES FOR OPTIMIZED ELEMENT

f	Γ_{goal}	η_{goal}
3.75 GHz	-4.3 dB	-2 dB
5 GHz	-6.8 dB	-1 dB
16 GHz	-6.8 dB	-1 dB
18GHz	-4.3 dB	-2 dB

In addition to the coefficients of the level set function, two other geometric parameters are allowed to vary during the optimization: the feed location o along the line of symmetry, and the thickness of the substrate t ($\varepsilon_r = 3.0, \tan\delta = 0.003$). The LSF used for this optimization consists of a 5x8 grid of basis functions with mirror symmetry. The periodicity of the element in both dimensions is 8.64 mm. These dimensions are depicted in Fig. 4(a).

B. Optimized Element

The LSF optimization converged (population fitness standard deviation $\sigma < 0.001$ after 7173 evaluations. The best candidate was the 6174th candidate to be evaluated, and the resulting surface pattern is shown in Fig. 4(c). The feed offset determined by the optimization was $o = 3.3\,\text{mm}$ and the thickness of the substrate likewise $t = 3.3\,\text{mm}$.

Up to this point we have reasoned based on intuition that the LSF might be more favorable for antenna optimization than the fragmented basis; this optimization provides an opportunity to support that claim. Of course, a rigorous comparison between stochastic optimization techniques is quite challenging and entirely outside of the scope of this work, but it is at least instructive to provide an anecdotal comparison between this optimization and those appearing in the literature, which likely represent a best effort. Prior work at GTRI [16], [17] has demonstrated a 4.7:1 bandwidth (1.435 GHz to 6.7 GHz) unbalanced aperture. While the actual bands of interest are different, the bandwidth and fitness function (scaled by frequency) are identical to the present work. Furthermore, the specific genetic algorithm used in this fragmented aperture array is identical to the GA used for LSF optimization.

The radiating surface patterns and performance of both the LSF and fragmented arrays are shown in Fig. 6, with simulated efficiency η and feed return loss Γ compared against the objective functions η_{goal} and Γ_{goal}, respectively. The fragmented results are scaled in frequency to match the LSF.

An immediate observation is substantial similarity between the fragmented and LSF patterns; both producing a nominally T-shaped element connected in the x-dimension. The LSF element is directly connected, while the fragmented element has strong capacitive coupling between neighboring elements. That being said, the LSF element produced has substantially lower complexity than the fragmented element, and the feature sizes in the fragmented array, originally optimized at lower frequencies, would be difficult to fabricate if scaled to this higher frequency band. Furthermore, the LSF shows superior performance to the fragmented element everywhere except the lowest portion of the band. These metrics are summarized in Table II.

With the usual caveat that the comparison of only two instances of a stochastic algorithm is little in the way of evidence

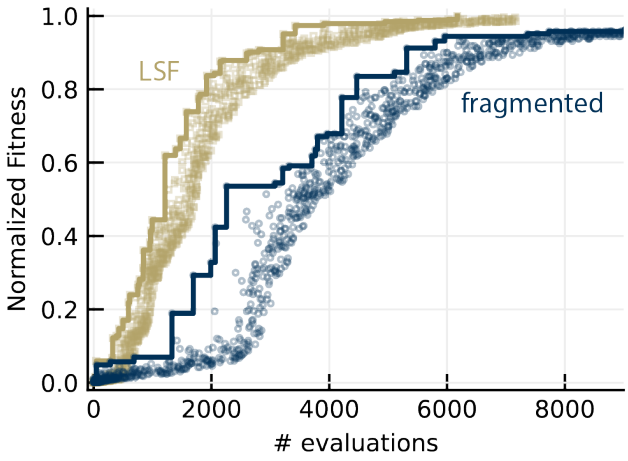

Fig. 6. Comparison of the convergence rate between LSF and fragmented optimizations using the genetic algorithm. The solid line indicates the best solution over time, while the markers depict the evolution of the entire population over time. Normalized fitness is $(\max\{\mathcal{F}\}/\mathcal{F})^2$.

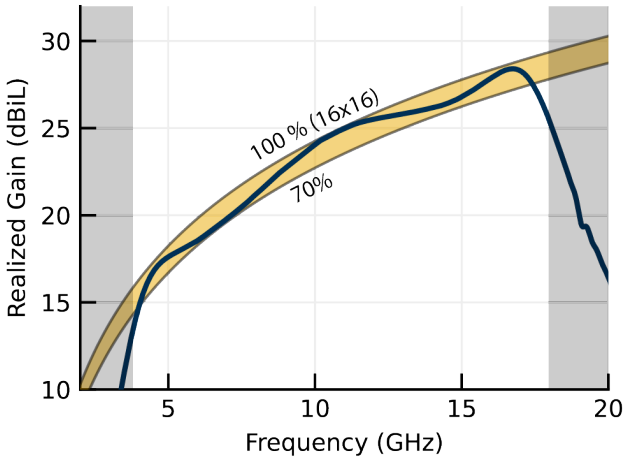

Fig. 7. Broadside gain of the 18x18 (16x16 driven) array, showing between 70% and 100% aperture efficiency compared to the 16x16 driven area.

for a claim, the comparison in algorithm convergence between LSF and fragmented optimizations is noteworthy. Both LSF and fragmented GA optimizations share similar crossover functions, and mutation for the fragmented case causes a bit flip for a random selection of fragments determined by the mutation rate, while mutation of a particular parameter in the LSF case is a Gaussian mutation with $(\mu = 0, \sigma = 1)$ over the parameter $\alpha_i \in [-1, 1]$. The convergence profile for each optimization is shown in Fig. 6. The presented curves are not a comparison of the final fitness value; as previously mentioned, the LSF case converged to a higher fitness value than did the fragmented case. It is instead a comparison of the rate at which the GA converged to that final fitness value, and for this reason we define a normalized fitness between 0 and 1 by:

$$\mathcal{F}_{\text{norm}} = \left(\frac{\max\{\mathcal{F}\}}{\mathcal{F}}\right)^2 \tag{5}$$

Note that this normalization changes the range of possible fitness values from $\mathcal{F} \in (-\infty, 0)$ to $\mathcal{F}_{\text{norm}} \in (0, 1)$.

TABLE II
FRAGMENTED VS. LSF COMPARISON (4–17.5 GHZ)

Metric		Fragmented	LSF
η	best:	-0.33 dB	-0.07 dB
	worst:	-2.37 dB	-1.64 dB
Γ	best:	-16.67 dB	-21.25 dB
	worst:	-3.86 dB	-5.6 dB

Two qualitative observations arise from this comparison. First, the LSF optimization begins immediately obtaining significant improvements in the fitness of the population as a whole, while the fragmented optimization evaluates over 1500 individuals with minimal improvements before finding a few better cases, and over 2400 evaluations before the population begins to converge to higher fitness values. Second, the LSF optimization more frequently finds incremental improvements; in the first 5000 evaluations in each optimization, 1015 individuals were added to the population (rather than being discarded) for the LSF optimization versus 685 individuals in the fragmented case, which signifies greater optimization efficiency with the LSF (in this case). These are factual observations without any conclusion attached; nothing more can be said definitively without further trials.

IV. Finite Array

We finally briefly turn to consideration of the optimized LSF element in a finite phased array. We model a 16x16 driven array with an extra boundary of dummy elements for a total of 18x18 elements (155.4 mm x 155.4 mm). The realized gain of this array is shown in Fig. 7. The efficiency at broadside ranges from 70% to 97.5% between 4.0 GHz to 17.4 GHz, resulting in a 4.35:1 bandwidth.

Scanning performance is calculated by simulated embedded element patterns for each driven element (256 simulations) and using those to synthesize steering. Steering along the elevation principal plane is shown in Fig. 8, and steering along azimuth is shown in Fig. 9. The elevation scan shows close to $\cos\theta$ scan loss, while the azimuth scan is nominally $\cos^2\phi$, with a slight scan blindness near 50 degrees.

V. Conclusion

The level set function offers a promising alternative to the fragmented basis for optimization-aided design of phased array elements. Complex features can be represented by only a few continuously variable parameters, the variation of which has a direct effect on the size of features at a particular location on the unit cell. Both symmetry and continuity are enforced by the periodic LSF, which enables the high degree of coupling necessary to realize broadband performance.

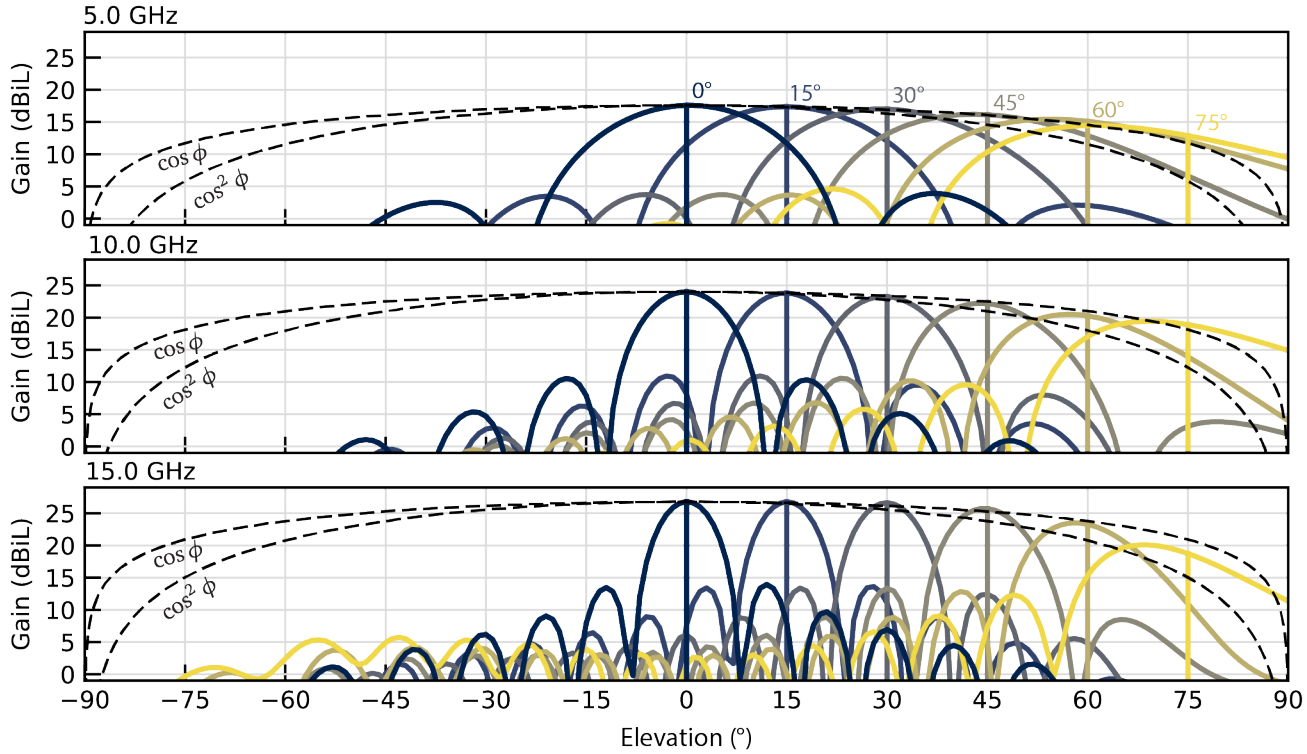

Fig. 8. Scan performance along the elevation principal plane. Each vertical line represents the desired scan angle (the scan angle predicted by the linear phase applied to the elements.)

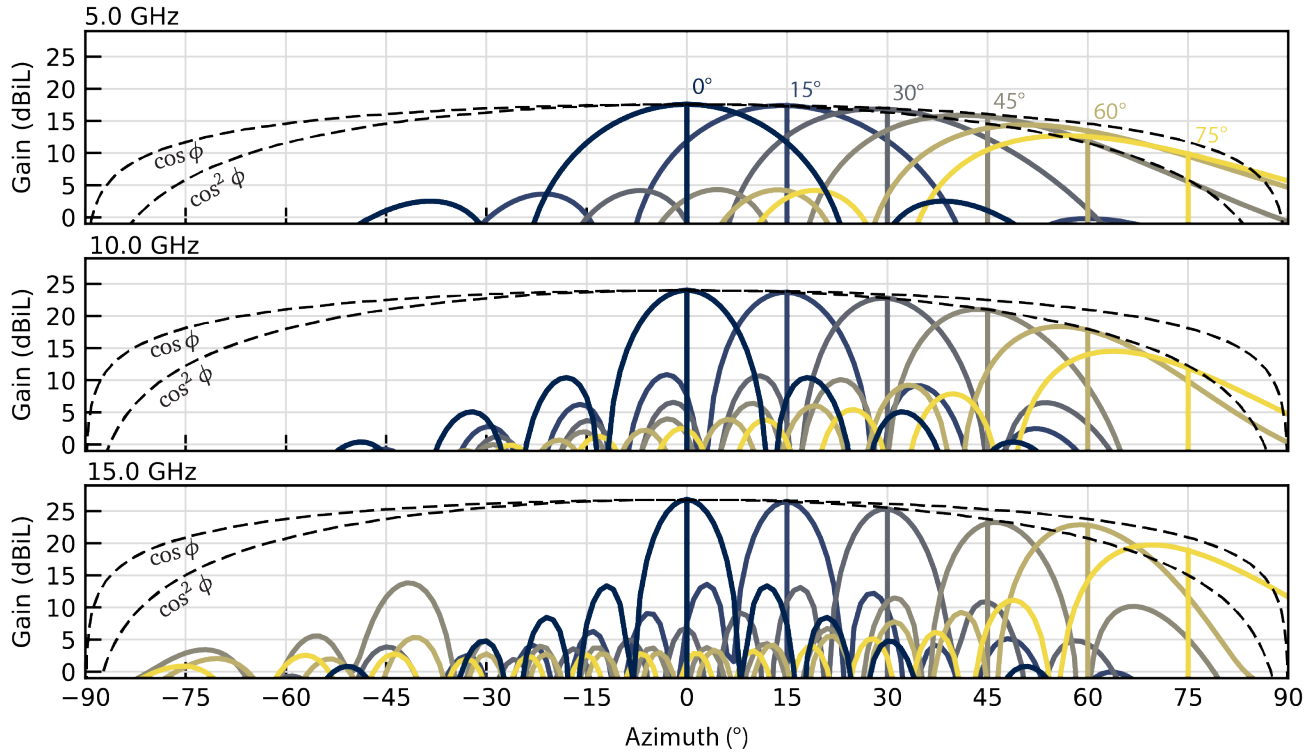

Fig. 9. Scan performance along the azimuth principal plane. Each vertical line represents the desired scan angle (the scan angle predicted by the linear phase applied to the elements.)

The smooth relationship between the continuous parameters and the metal pattern corresponding to them results in an improved optimization landscape. A comparison between a previously optimized and published fragmented aperture provides compelling support for improved convergence speed and better final designs over the fragmented aperture. The design produced from an LSF optimization demonstrates efficiency of 70-97.5% over a 4.35:1 bandwidth. Scanning a 16x16 array with an added perimeter of dummy elements shows good scan performance out to 75 degrees in elevation and to 45 degrees in azimuth.

Several opportunities exist to further this work. First, a substantially more robust comparison between the fragmented aperture antenna and the LSF array would be instructive in determining the circumstances in which one is to be preferred over the other, if at all. The comparisons briefly considered here only form one anecdote for a specific selection from a diverse set of possible antenna requirements, some of which might be better served by the fragmented array. A robust comparison would require the exploration of multiple applications with many optimizations run in sequence with a variety of starting conditions and optimization parameters.

Second, the results in this study have been produced merely from simulation, and ought to be supported by measurement. Fabrication of the 18x18 array studied in this work, or even a smaller array paired with additional simulations, would go far in confirming the validity of this design technique, as well as assessing the success of the material distribution function in applying fabrication constraints to the design. Improved fabrication constraint algorithms are also needed.

Finally, the phased array element designed in this study is close to the minimum complexity possible for a phased array – single-layer, unbalanced, no vias, no impedance matching or parasitic layers, and no attempts at surface wave suppression. In short, none of the usual strategies for improving the bandwidth and scan volume of the element have been applied. While this teases the idea that performance of the element can only be improved, it provides no insight into the most effective away to incorporate those strategies into the optimization. In a similar vein, future work could expand the p-LSF optimization approach to defining the metallization on more complex array architectures such as the BAVA, PUMA, TCDA, etc. for improved ultra wideband antenna performance.

ACKNOWLEDGMENT

The authors thank Dr. R. Todd Lee for providing guidance on some of the array analysis presented in this work, and Mr. Daniel J. P. Dykes for providing historical optimization data for the fragmented aperture array. In addition, the support provided by GTRI's Independent Research and Development program was instrumental in developing this optimization technique.

REFERENCES

[1] S. S. Holland and M. N. Vouvakis, "The Planar Ultrawideband Modular Antenna (PUMA) Array," *IEEE Transactions on Antennas and Propagation*, vol. 60, no. 1, pp. 130–140, Jan. 2012.

[2] M. W. Elsallal, J. R. Hood, and R. Kindt, "Development of substrate-free frequency-scaled ultra-wide spectrum element (FUSE) phased array," in *2016 IEEE International Symposium on Phased Array Systems and Technology (PAST)*, Oct. 2016, pp. 1–5.

[3] M. Hamza, C. L. Zekios, and S. V. Georgakopoulos, "An Ultra-Wideband Fully-Planar Inverted-L Monopole (FILM) Array," in *2022 IEEE International Symposium on Phased Array Systems & Technology (PAST)*, Oct. 2022, pp. 1–6.

[4] I. Tzanidis, K. Sertel, and J. L. Volakis, "Interwoven Spiral Array (ISPA) With a 10:1 Bandwidth on a Ground Plane," *IEEE Antennas and Wireless Propagation Letters*, vol. 10, pp. 115–118, 2011.

[5] Y. Rahmat-Samii, J. M. Kovitz, and H. Rajagopalan, "Nature-inspired optimization techniques in communication antenna designs," *Proceedings of the IEEE*, vol. 100, no. 7, pp. 2132–2144, 2012.

[6] J. M. Kovitz, J. P. Santos, Y. Rahmat-Samii, N. F. Chamberlain, and R. E. Hodges, "Enhancing communications for future mars rovers: Using high-performance circularly polarized patch subarrays for a dual-band direct-to-earth link," *IEEE Antennas and Propagation Magazine*, vol. 59, no. 4, pp. 50–61, 2017.

[7] O. Sigmund and K. Maute, "Topology optimization approaches," *Structural and Multidisciplinary Optimization*, vol. 48, no. 6, pp. 1031–1055, Dec. 2013.

[8] P. Friederich, L. Pringle, L. Fountain, P. Harms, D. Denison, E. Kuster, G. Smith, J. Maloney, and M. Kesler, "A New Class of Broadband Planar Apertures," in *Proceedings of the 2001 Antenna Application Symposium - Volume II*, Monticello, IL, Sep. 2001.

[9] A. Saad-Falcon, C. Howard, J. Romberg, and K. Allen, "Level set methods for gradient-free optimization of metasurface arrays," *Scientific Reports*, vol. 14, no. 1, p. 16674, Jul. 2024.

[10] M. F. Schubert, A. K. C. Cheung, I. A. D. Williamson, A. Spyra, and D. H. Alexander, "Inverse Design of Photonic Devices with Strict Foundry Fabrication Constraints," *ACS Photonics*, vol. 9, no. 7, pp. 2327–2336, Jul. 2022.

[11] R. E. Christiansen and O. Sigmund, "Inverse design in photonics by topology optimization: Tutorial," *JOSA B*, vol. 38, no. 2, pp. 496–509, Feb. 2021.

[12] J. G. Maloney, B. N. Baker, R. T. Lee, G. N. Kiesel, and J. J. Acree, "Wide scan, integrated printed circuit board, fragmented aperture array antennas," in *2011 IEEE International Symposium on Antennas and Propagation (APSURSI)*. Spokane, WA: IEEE, Jul. 2011, pp. 1965–1968.

[13] A. Ellgardt and P. Persson, "Characteristics of a broad-band wide-scan fragmented aperture phased array antenna," in *2006 First European Conference on Antennas and Propagation*. Nice, France: IEEE, Nov. 2006, pp. 1–5.

[14] B. Thors, H. Steyskal, and H. Holter, "Broad-band fragmented aperture phased array element design using genetic algorithms," *IEEE Transactions on Antennas and Propagation*, vol. 53, no. 10, pp. 3280–3287, Oct. 2005.

[15] D. J. P. Dykes, K. M. Bowland, and K. W. Allen, "Wideband millimeter-wave fragmented aperture antenna," in *2017 IEEE National Aerospace and Electronics Conference (NAECON)*. Dayton, OH: IEEE, Jun. 2017, pp. 213–216.

[16] D. W. Landgren, D. J. P. Dykes, and K. W. Allen, "Aa Unbalanced Feed Design for Wideband Phased Arrays," Jun. 2017.

[17] D. Landgren, G. Smith, T. Brunasso, K. Allen, D. Dykes, J. Kovitz, J. Perez, J. Dee, J. Marsh, and C. Hunter, "A Broadband Array with Unbalanced Feeds : Elements and Power Combiners Based on the Fragmented Aperture Principle," in *2019 IEEE International Symposium on Antennas and Propagation and USNC-URSI Radio Science Meeting*. Atlanta, GA, USA: IEEE, Jul. 2019, pp. 1223–1224.